Deviation of the Shape of Bennu from Rotational Figures of Stability

J.H. Roberts[1], O.S. Barnouin[1], C.L. Johnson[2,3], M.G. Daly[4], M.E Perry[1], R.T. Daly[1], M.M. Al Asad[2], E.E. Palmer[3], J.R. Weirich[3], P. Michel[5], W.F. Bottke[6], K.J. Walsh[6], M.C. Nolan[7], D.J. Scheeres[8], J.W. McMahon[8], G.A. Neumann[9], D.S. Lauretta[7], and the OSIRIS-REx Team.

[1]The Johns Hopkins University Applied Physics Laboratory; [2]Department of Earth, Ocean and Atmospheric Sciences, University of British Columbia; [3]Planetary Science Institute; [4]The Centre for Research in Earth and Space Science, York University; [5]Observatoire de la C'ôte d'Azur, University of Nice; [6]Southwest Research Institute; [7]Lunar Planetary Laboratory, University of Arizona; [8]Colorado Center for Astrodynamics Research, University of Colorado. [9]NASA Goddard Space Flight Center.

Introduction

- Images of asteroid (101955) Bennu acquired by the OSIRIS-REx mission [1] reveal a rocky world covered in rubble.
- Shape deviates from hydrostatic surface [2]
  - Internal friction and/or cohesion even if no tensile strength [3,4]
- Understanding the deviation of the surface from idealized shape may help constrain mechanical properties of the interior
- Geologic evolution of Bennu is driven by downslope migration of surface material [5] and rubble.
  - May be caused by YORP-induced spin-up [e.g., 6,7], re-accumulation [8, 9], impact-induced seismic shaking, thermal stresses, or tidal disruption by close encounters to larger bodies.

Equilibrium figures

Maclaurin Spheroid

- Simplest model of rotating figure
- Oblate spheroid which arises when a fluid, self-gravitating body of uniform density ρ rotates with constant angular velocity Ω.
  - Reasonable assumptions for small rubble pile asteroid
- Here, generalized to cohesionless solids [10] with internal friction angle ϕ.
- **We are interested in the deviation of these bodies from the idealized surfaces**
- Maximum stable spin rate is function of ϕ and ratio α of length of polar axis (c) to length of equatorial axis (a):

$$\frac{\Omega^2}{\pi G\rho} = \frac{2\alpha\sqrt{m+2\alpha^2}}{m(1-\alpha^2)^{3/2}}\cos^{-1}\alpha - \frac{2(m+2)\alpha^2}{m(1-\alpha^2)}, \quad m = \frac{(1+\sin\phi)}{(1-\sin\phi)}$$

- Five asteroids for which we have high-resolution shape models (Table 1) have been approximated as Maclaurin spheroids and plotted on Fig. 1a.
- Strengthless body is rotationally stable if it plots below the lowest curve on Fig. 1a.

- Adding internal friction helps it hold together at higher rotation rates (Fig. 1a)
- An object with the observed rotation rate and density (see Table 1) of **Bennu [11,12] requires ϕ > 18° to prevent further flattening**, despinning and potentially undergoing binary fission.

Prolate Spheroid

- More complicated function of allowable Ω as function of α and ϕ,
  - Both upper AND lower bounds on Ω.
- Five asteroids for which we have high-resolution shape models (Table 1) have been approximated as prolate spheroids and plotted on Fig. 1b.
- All prolate bodies require internal friction or cohesion

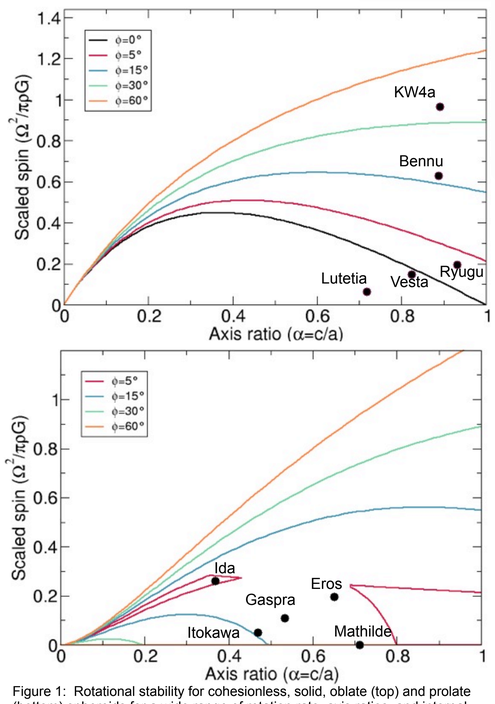

Figure 1: Rotational stability for cohesionless, solid, oblate (top) and prolate (bottom) spheroids for a wide range of rotation rate, axis ratios, and internal friction angles: The curves of rotational stability for cohesionless, solid, oblate spheroids for a wide range of rotation rate, oblateness, and internal friction. Each curve describes the limits of the allowable dimensionless rotation rate as a function of the axis ratio. Each point marks the dimensionless spin rates and axis ratios consistent with observed asteroids (Table 1).

Results for Bennu

- Shape model developed from SPC [13] (derived from images taken during Preliminary Survey and Orbital A phases [1]), validated by limb measurements, and further constrained by OLA [2,14].
- Figure 2 shows height of shape model above the equilibrium spheroid consistent with Bennu's parameters.
  - Spherical harmonic decomposition shows strong degree 4 contribution (Figure 3, [15]). Zonal component is largely due to the equatorial ridge, but there is also a strong sectoral component "Squarish" shape seen in the polar views. Four N-S trending ridges are outlined in Figure 2.
- Figure 4 shows the tilts, which further constrain ϕ
  - Internal friction must be high enough to support material from sliding downslope to meet the equilibrium surface
  - Maximum tilts are at lower latitudes than those on a MacLaurin surface; slopes of the equatorial ridge

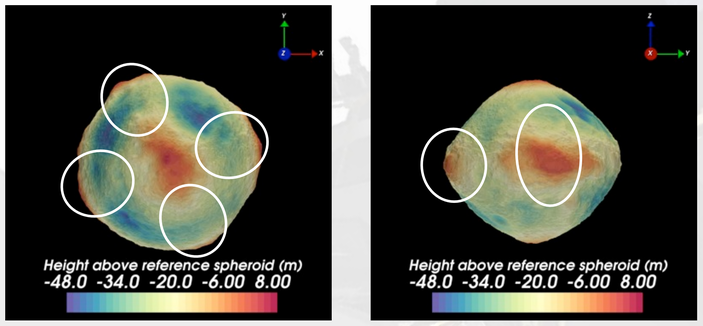

Figure 2: Deviation of Bennu's shape model from the closest-fit Maclaurin spheroid consistent with Bennu's observed density (1.19 g cm^{-3}) and rotation period (4.3 h). Left: Polar view. Right: Equatorial view. Ellipses mark portions of the north-south ridges, which are clearly high-standing relative to locations to the east and west.

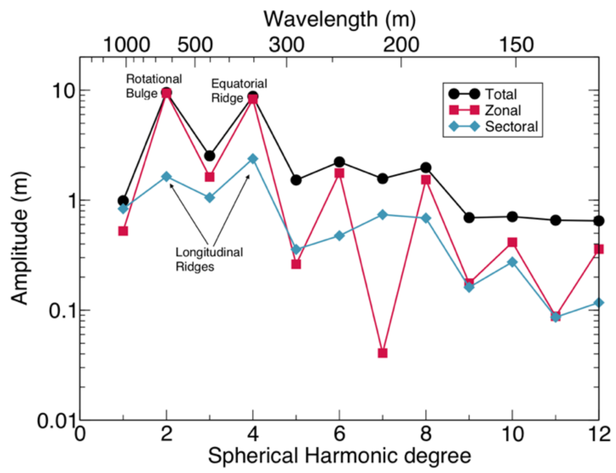

Figure 3. Amplitude spectrum of a spherical harmonic expansion for the shape model The large zonal degree 2 and 4 terms show the most distinctive characteristic of Bennu: the top shape with an equatorial ridge. The relatively low amplitudes of the degree 3 and 5 terms demonstrate that there is no substantial north-south asymmetry in Bennu's shape. The degree 4 sectoral terms (C44 and S44), capture the ~90° longitudinal variations in shape associated with the major north-south ridges.

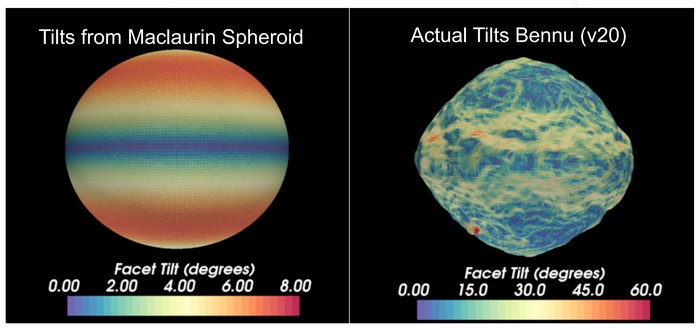

Figure 4: Tilts (angle between the normal to the surface and the direction to the center) from closest-fit Maclaurin spheroid consistent with Bennu's observed density and rotation period (left), and from the shape model (right).

Results for other Asteroids

- Repeated analysis for 10 asteroids in Table 1.
- Oblate body tilts peak ~10°
- Prolate body tilts peak ~20°
- Both much higher than idealized shape
- Very long tails at upper ends

Asteroid	Spheroid	α	Ω (s^{-1})	ρ (g cm^{-3})
4 Vesta	Maclaurin	0.8242	3.27×10^{-4}	3.456
21 Lutetia	Maclaurin*	0.7182	2.14×10^{-4}	3.4
243 Ida	Prolate	0.3679	3.77×10^{-4}	2.6
253 Mathilde	Prolate	0.7121	4.18×10^{-6}	1.3
433 Eros	Prolate	0.6512	3.31×10^{-4}	2.67
951 Gaspra	Prolate	0.5330	2.48×10^{-4}	2.7
25143 Itokawa	Prolate*	0.4701	1.44×10^{-4}	1.95
66391 1999 KW4a	Maclaurin	0.8907	6.31×10^{-4}	2
101955 Bennu	Maclaurin	0.8874	4.07×10^{-4}	1.19
162173 Ryugu	Maclaurin	0.9317	2.29×10^{-4}	1.27

Table 1: Physical properties relevant to rotational stability of ten asteroids, here approximated as either oblate or prolate spheroids. Asteroids denoted by * are better approximated as tri-axial ellipsoids, but for this comparison have been classified as oblate or prolate.

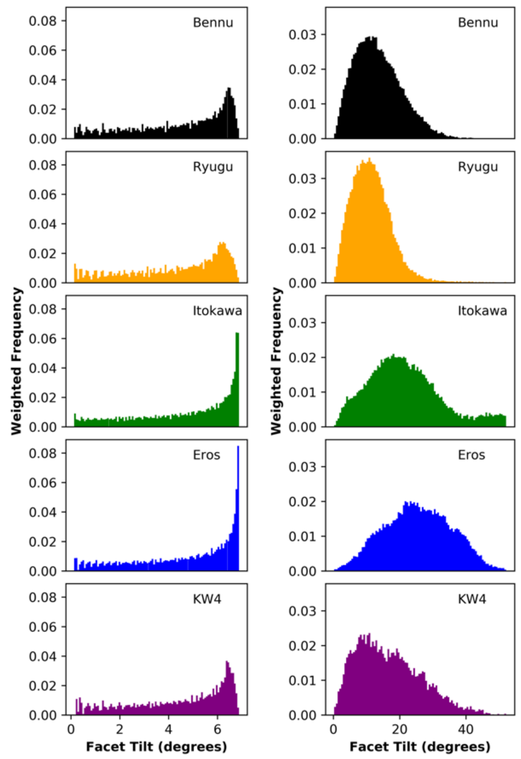

Figure 5: Histograms showing the distribution of tilts on closest-fit Maclaurin or prolate ellipsoids to the shapes of Bennu, Ryugu, Itokawa, Eros, and KW4a (left), and on shape models of these asteroids (right).

Discussion

- Equatorial ridges and N-S ridges clearly visible in height difference map
  - May point to underlying structure – few large fragments controlling shape?
- Does the equatorial ridge act as a barrier?
  - It's a gravitational minimum, so rubble slides downhill to it.
  - May have some larger blocks (buried in fines) there
  - Additional material may be lodged up against the ridge?
- Systematic variation in tilt distribution for oblate vs. prolate asteroids
- Many asteroids better represented as triaxial ellipsoids. Requires numerical modeling.
- Stability analysis assumes internal friction is the only source of strength. Cohesion would reduce the required friction angle.

References

[1] DellaGiustina, D. et al. (2018), AGU Fall Meeting P21A-04. [2] Barnouin, O.S. et al. (2019) LPSC 50, 1744. [3] Zhang, Y. et al., (2017) Icarus 294, 98–123. [4] Hirabayashi, M. and Scheeres, D.J. (2015) ApJ Letters, 798, L8. [5] Richardson, J.E. and Bowling, T.J. (2014) Icarus 234, 53–65. [6] Rubincam, D.P. (2000) Icarus, 148, 2–11. [7] Walsh, K.J., et al., (2008) Nature, 454, 188–191. [8] Michel, P. et al. (2001) Science, 294, 1696–1700. [9] Michel, P. et al. (2019) LPSC 50, 1659. [10] Holsapple, K.A. (2004) Icarus 172, 272–303. [11] Palmer, E. et al. (2019) LPSC 50, 2588. [12] Scheeres, D.J. et al. (2018) AGU Fall Meeting P22A-05. [13] Gaskell, R.W. et al. (2008) MAPS, 43, 1049–1061. [14] Daly, M.G. et al. (2017) SSR, 212, 899–924. [15] Barnouin, O.S. et al. (2019), Nature Geosci., in press.